ICSO 2016

International Conference on Space Optics

Biarritz, France

18–21 October 2016

Edited by Bruno Cugny, Nikos Karafolas and Zoran Sodnik

Influence of the Exomars 2016 lander elements in the uncertainty of irradiance measurements for the dreams-SIS instrument

F. J. Alvarez-Ríos

J. J. Jiménez

V. Apestigue

I. Arruego

et al.

esa icso proceedings cnes

International Conference on Space Optics — ICSO 2016, edited by Bruno Cugny, Nikos Karafolas, Zoran Sodnik, Proc. of SPIE Vol. 10562, 105625B · © 2016 ESA and CNES
CCC code: 0277-786X/17/$18 · doi: 10.1117/12.2296141

INFLUENCE OF THE EXOMARS 2016 LANDER ELEMENTS IN THE UNCERTAINTY OF IRRADIANCE MEASUREMENTS FOR THE DREAMS-SIS INSTRUMENT.

F.J Álvarez Ríos[1], J. J. Jiménez[1], V. Apestigue[1], I. Arruego[1], I. Martin[1], L.M Sanchez-Brea[2]
[1]*Instituto Nacional de Técnica Aeroespacial – INTA, Spain*
[2] *Applied Optics Complutense Group, Optics Department,*
Facultad de Ciencias Físicas, Universidad Complutense de Madrid, Spain

I. INTRODUCTION

DREAMS SIS is an optical radiometer that will provide measurement of the sun irradiance on the Mars surface [1],[2],[3]. The instrument will be on board as payload of the EDM, (Entry and Descend module) of EXOMARS 2016 ESA [4] mission showed in Fig. **1**a. (Courtesy of ESA). The radiometer is miniaturized and multi-channel radiometer based on Schott filters, interference filters and Si-photodiode detector to make spectrally measurements in the wavelength range of UVA (315-400 nm) NIR (700-1100nm) and a global range (silicon detector) between 200 nm and 1200 nm. A top view of the detector it is shown in Fig. **1**b. The global channel is pointed to the zenith. The NIR and UVA channels are repeated in the lateral facets with azimuthal distribution (120º between each facet). For the lateral facets case, the optical channels are pointed 60º respect to the zenith point. Each facet has been identified using the azimuth Earth orientation (North-South and West-East). The theoretical field of view (FOV) of the DREAMS instruments is the next: 90º for the Total Channel, 38º for the UVA Channel and 45º for the NIR Channel.

Some elements of the EXOMARS 2016 lander, like fuel balls and pipes are interfering with the FOV of the DREAMS SIS. These interferences, see Fig. 1c, could produce Stray-light [5] due the Sun light reflections into the optical sensor, affecting the signal(S^A_{Total}) measured by the detector. This signal is proportional to the sum of the irradiance flux for the diffuse (S^A_{Diff}) and direct (S^A_{Direct}) solar irradiance contributions. The reflections will introduce an uncertainty solar irradiance measurements, δS^A_{Direct} and δS^A_{Diff}.

Two approaches have been performed to estimate the amount of undesired signal reaching to the sensor. One of them, was the use of ray-trace technique, in order to simulate the possible reflections in a 3-D Model of the lander. Simulations have been performed to:

- Identify the lander elements that will contribute to the sun reflections into the optical channels.
- Estimate δS^A_{Direct} and δS^A_{Diff}.
- Get an uncertainty map of the reflections in terms of the solar angle coordinates (Azimuth, Zenith) for each channel.
- Daylight simulations, combining direct irradiance and the diffusive 2-D sky radiances through different sun trajectories.

The other approach to evaluate the reflections consisted into developing a physical model of the lander. The model has been used in combination with the FCM (field campaign model) of the DREAMS-SIS, that is a replica of the Flight Model. Experimental measurements were carried out in order to verify the simulations in the terrace of the INTA Optoelectronics laboratory.

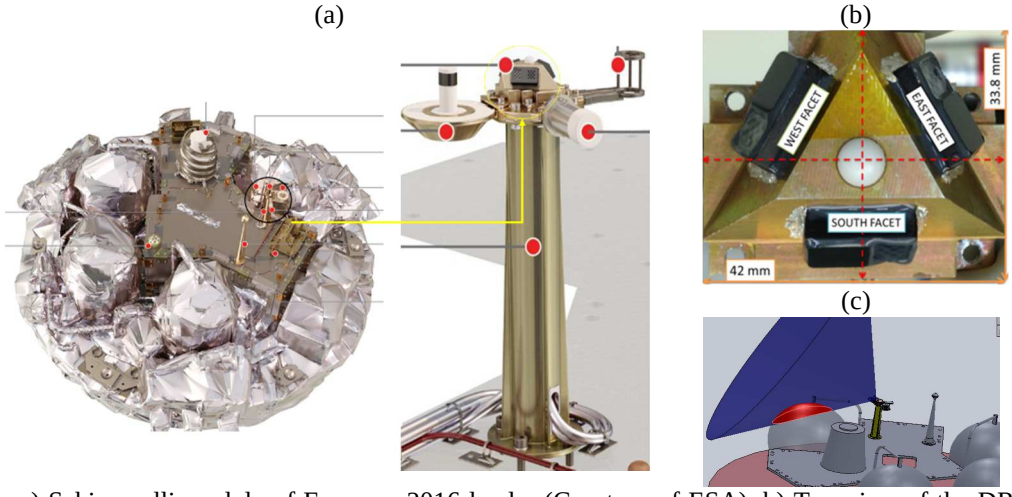

Fig. 1: a) Schiaparelli module of Exomars 2016 lander (Courtesy of ESA). b) Top view of the DREAMS-SIS optical channels) Interference of one of the channels with one element of the Exomars 2016 lander (CAD-View)

II. RAY-TRACE SIMULATIONS

The 3-D model Fig. 2 presents the most representative elements that are assumed to produce reflections like the fuel balls and pipes. For the EDM, the material employed to cover the elements is aluminized kapton. This material optical behavior is almost specular [6],[7]. During the simulations, the materials of the lander have been considered as specular with a reflectivity of 80%. The model was surrounded by a hemisphere that represents the sky dome. This Sky dome, is the source from the rays is traced up to the sensor.

(a) (b)

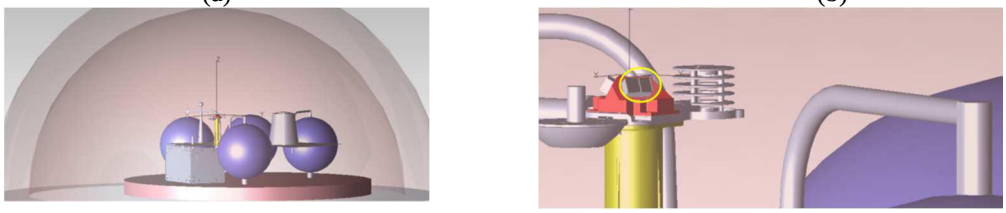

Fig. 2: 3-D CAD view employed for the ray-trace simulation.

A. SKYLINE MAP

The first step for the simulations was to determine the view factor of the sensor. It allows the detection of the objects inside the optical FOV of DREAMS-SIS channels. The procedure consists of the following:

Firstly, the rays are traced from the sky dome to the detector. For this simulation the sky radiance of the sky dome has been considered uniform. Once the rays are traced, the information about the director cosine of the rays and the nature of the rays (direct or reflected rays) are stored. The cosine director coordinates of the rays are translated to Azimuth and Zenith angle coordinates. The representation of the direct rays reaching to the sensor optical entrance is showed in Fig. **3**a for the case of the DREAMS-SIS NIR South Facet, whereas the rays reflected by the EDM elements are showed in Fig. **3**b It can be seen that part of the fuel balls and pipe are inside the FOV of the NIR facet channels. We have called this representation "Sky-line map".

Following, it is important to note that the simulated rays only reach the entrance of the optical system (see Fig. 2b). Instead of simulate the internal optical system; the stored rays from the simulation are weighted by the angular response function of the instrument (ARF). The ARF has been measured for each channel in the laboratory. The angular calibration consists on automatic 2-D angular sample of the solar angles positions (azimuth and zenith angles) under a reference light source [8].

Fig. 3c and Fig. 3d present the Sky-line after weight the representation by the ARF for the direct rays and reflected ray respectively. It can be seen that the lander interference are reduced highly due the action of FOV channel.

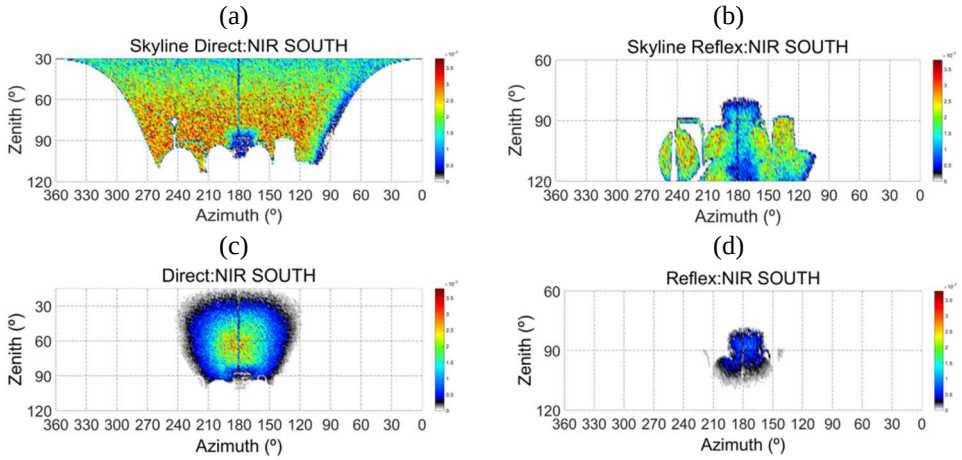

Fig. 3: Sky-line map representation for the NIR South facet channel. a), b) Direct and reflected rays reaching the entrance of the optical system. c), d) Direct and Reflected rays weighted by the ARF channel function

B.DIFFUSIVE CONTRIBUTION TO THE UNCERTAINTITY

The uncertainty estimation for diffusive contribution of the signal (δS^A_{Diff}) has been evaluated for the case of Uniform sky radiance. We estimate the parameter as:

$$\delta S^A_{Diff}(\%) = \frac{\int_0^{2\pi}\int_0^{\alpha} SKY^{reflex}\, d\alpha d\theta}{\int_0^{2\pi}\int_0^{\alpha} SKY^{Direct}\, d\alpha d\theta} \quad (1)$$

Where SKY^{reflex} and SKY^{Direct}, are the Sky-line representation for an optical channel weighted by the ARF channel for the reflected and direct rays respectively. The results are listed in Table 1:

Table 1: Results for δS^A_{Diff}

Sensor	δS^A_{Diff}
NIR West	2.11%
UV West	0.79%
NIR East	0.15%
UV East	0.11%
NIR South	6.08%
UV South	4.12%
TOP	0.87%

C. DIRECT CONTRIBUTION TO THE UNCERTAINTITY

The key point to estimate δS^A_{Direct}, is to find solar angles positions (zenith, azimuth) where the sun rays are reaching to the sensor directly and reflected at the same time. In this case, the simulation process is reversed, so the rays are traced back from the sensor up to Sky dome. The procedure is listed below:

1) Reversed rays are traced from the sensor are weighted by the ARF of each channel up to the Sky dome.
2) Store cosine director and flux of the traced rays.
3) Generate a matrix of solar position of 1º Step and size 360x120 (azimuth (θ) and zenith (α) angles). Two matrixes are generated one for the direct rays and the other one for the reflected.
4) δS^A_{Direct} is estimated dividing the matrix generated for the direct case (M_{direct}) and reflection case ($M_{reflected}$) according to:

$$\delta S^A_{Direct} = \frac{M_{reflected}(\alpha,\theta)}{M_{direct}(\alpha,\theta)} \quad (2)$$

Fig. 4 schematizes the process described before for the NIR West faced case. In Fig. 4.a is shown the reversed ray trace up to the Sky dome the right image correspond to the direct/reflected rays. The matrix of solar positions has been filled out with the ray information. In Fig. 4.b is represented the division of the matrixes in order to calculate the perceptual error of δS^A_{Direct}.

For these simulations, the NIR West faced was the channel with the higher δS^A_{Direct}. Anyway, the values where the uncertainty is above 15% are located in the angular positions where the ARF value is close to the 1% respect to the maximum. At this value, the signal it is not significant and the error introduced by the ARF are large.

(a) (b)

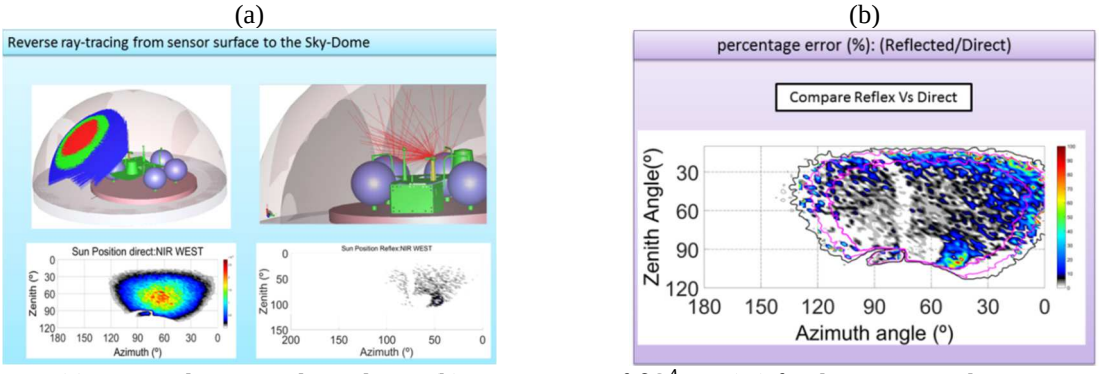

Fig. 4: (a) Reversed ray traced simulation (b) Matrix error of δS^A_{Direct} (%) for direct sun irradiance

D. 2D SKY RADIANCE

The diffuse solar radiation is not uniform across the sky dome. The intensity and spatial light distribution depend on sky conditions like dust deposition, clouds, humidity, etc. The Perez Sky radiance model [9] and the ISO/CIE standard general skies model [10] allow simulating different illuminances from totally overcast to clear sky conditions.

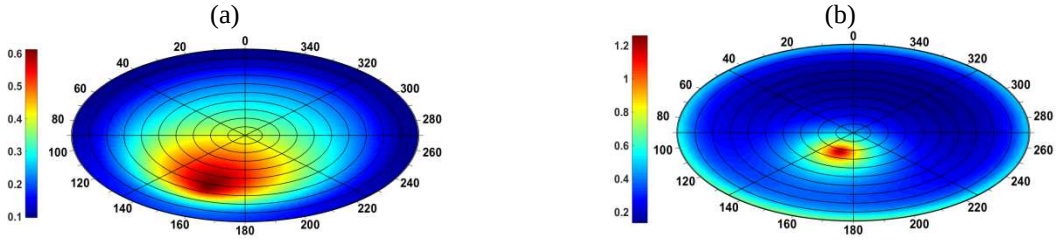

Fig. 5: Sky dome radiance simulation a) Overcast case b) Cloudless turbid case

The Sky radiance distribution for two different cases is shown in Fig. 5. Fig. **5**a represents an Overcast and slight brightening towards the sun case, where the solar angles are (60º, 160º) for the zenith and azimuth angles respectively. Fig. **5**b the case is for a cloudless turbid day with broad solar corona. The solar angles position are (25º, 160º) for the last case.

The model employed depends on the next parameters: Ψ (scattering angle), the solar zenith angle (ϕ_{sun}) and azimuth angle (θ_{sun}), and the angular position sky element (ϕ^*) and (θ^*) where are the zenith and azimuth angles respectively. The expression for the model is the next:

$$\Psi = \arccos[\cos(\phi_{sun})\cos(\theta^*) + \sin(\phi_{sun})\sin(\theta^*)\cos|\theta^* - \theta_{sun}|] \quad (2)$$

$$F(\Psi, \phi_{sun}) = [1 + a\exp(\frac{b}{\cos(\phi_{sun})}][1 + c\exp(d\cdot\Psi) + e\cos^2(\Psi)] \quad (3)$$

Where a,b,c,d,e are parameters models to fit for the different sky radiance conditions.

E. DAYLIGHT SIMULATION

In order to complete a day simulation and verify the evolution of the lander reflections, it is necessary to perform the solar trajectory of the sun across the sky dome. The direct and diffuse light has been simulated independently. In the direct light case a planar cylinder surface source has been introduced in the 3D Cad Model to trace the rays. On the other side, the Sky dome it is the source for the diffuse case simulations. The rays traced are weighted by the Sky radiance model explained in subsection 2.D for each pair of coordinates(ϕ_{sun}, θ_{sun}) of the solar trajectory.

Finally, In order to perform the simulations it is necessary to know the relative Irradiance value of the direct irradiance versus the diffuse. This value depends of the wavelength band of study (Global, UVA or NIR), solar position and atmospherically parameters. The SMART2 [11], [12] software that is atmospherically radiative transfer program has been employed for that proposal. It predicts the direct beam, diffuse and global irradiance on Earth surface. The relative variation for the NIR channels it is shown in Fig. 6. The orientation of the instruments has been set pointing the instrument south facet pointing to the south.

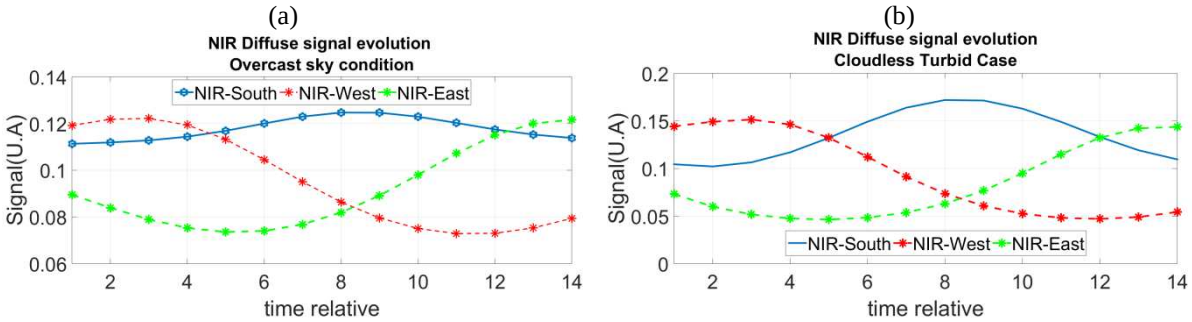

Fig. 6: Sky dome radiance trajectory simulation: a) Overcast case b) Cloudless turbid case

As example, the daylight trajectory reflections were simulated using the trajectory for one of the mission day.

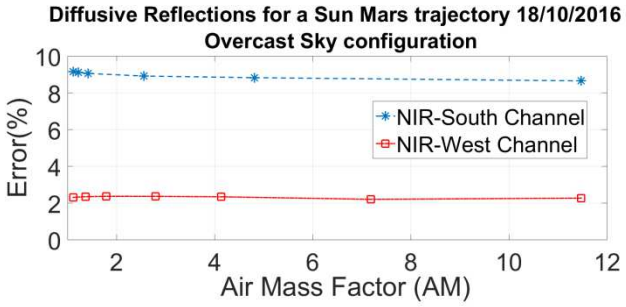

Fig. 7: Error (%) reflections estimated for an overcast Sky condition for the NIR-South and NIR-West channels.

III. EXPERIMENTAL MEASUREMENTS

The mock-up has been designed to perform the experimental validation. It contains the most representative elements that produce reflections according the simulations. To perform a complete study like for example: validate the simulations, finding specific reflections and simulate different landing orientation the mock-up was designed to provide the possibility to be tilted for the Z-axis and the Y-axis using a goniometric wedge.

A. SAMPLING OF DIRECT CONTRIBUTION UNCERTAINTY

The idea of this test is to sample the matrix error of Fig. **4**.b. The tested facet was the West facet. This facet has a fuel ball in front of the sensor and according to the simulations; This facet was affected by the direct and diffuse reflections during the simulations. The procedure was the next: The instrument is set horizontally, then, the west face is aligned pointing towards to the sun. Finally, the goniometric wedge (Fig. 8.b) start to make zenith sweeps between -40º up to 40º. The scanning was performed automatically for time duration between 15-20 minutes of duration. During the analysis, the relative movement of the sun respect the lander was taken in account deriving the final sunlight incident angle. The process is repeated three times. For each time, the material of the fuel was changed (black, Mylar and White(diffuse).

B. DIRECT AND DIFFUSE CONTRIBUTION POINTING TO THE SUN

This test consisted of pointing one of the facets measuring to the direct and diffuse side of the sky dome and appreciate visually a reflection coming back to the sensor, Fig. **8**.c. The identification of the reflections has been performed visually and only was possible when the fuel ball was surrounded by the Mylar material. The test was made for the West facet again. The materials employed to cover the fuel ball were: black, White (diffusive) and Mylar.

The time measurement was minimized in order to assume the sun was fixed during the measurements between the different materials. The times spend between materials measurements was less than 2 minutes.

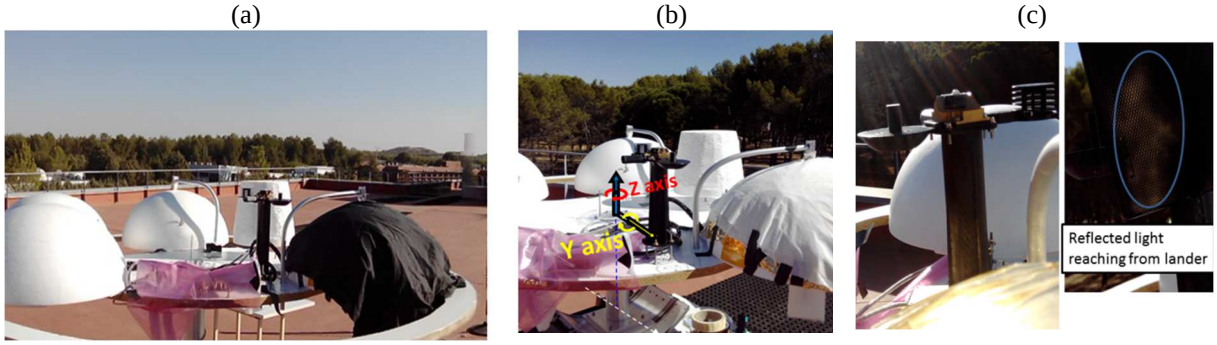

Fig. 8: Different mock-up views (a) General view, (b) Axis rotation of the model, (c) Sun light reflection reaching to the West facet channel.

C. RESULTS FROM TESTS

The Mylar and white (diffusive) balls were compared with the black ball case. The material employed to cover the ball in the black case, was an optical black blanket.

For the case of subsection III.A. The solar trajectories scanning are shown Fig. 9(a). The results are shown in Fig. 9(b) and Fig. 9(c). The signal deviation respect the black ball configuration for the other cases are below than 5% of error. Taking in account the instrument orientation were done visually, the results are inside the error due de orientation.

In the case subsection III.B. For the diffuse sun pointing case (δS^{A}_{Diff}), the comparison between the White and Black ball conditions is the worst case, with a relative mean difference of 15%. The real case with the ball surrounded by Mylar the mean difference is 3.6%. For the direct sun pointing case (δS^{A}_{Direct}), the reflections for any case are below than 1%. The results are listed in Table 2.

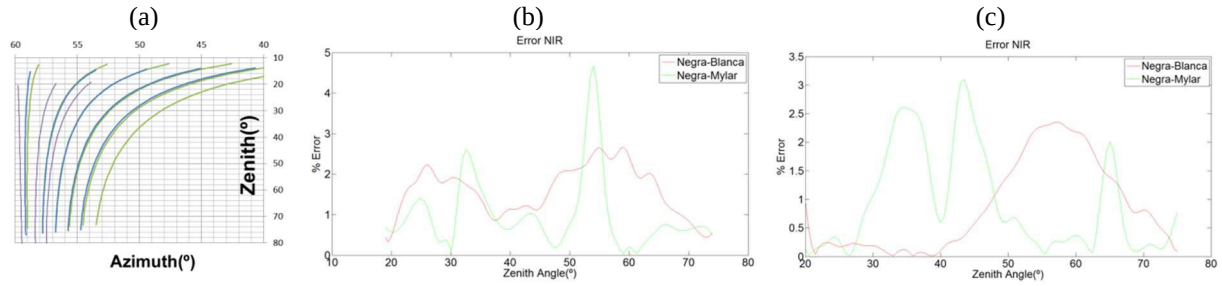

Fig. 9: (a): Solar coordinates for the DREAMS SIS. (b),(c): δS^{A}_{Direct} Relative error evolution of the signal for the White ball (red line) and Mylar ball (green line) respect the black ball for the NIR West facet Channel.

Table 2: Results for the optical test of III.B. W(White), B(black), M(Mylar)

NIR WEST CHANNEL

	Time	Black	White	Mylar	% W/B	% M/B
Diffuse Side	10/09/2014 8:37	5.24E-06	5.88E-06	4.94E-06	12%	6%
	10/09/2014 12:40	5.01E-06	5.84E-06	5.05E-06	17%	1%
	15/09/2014 9:15	4.30E-06	4.94E-06	4.47E-06	15%	4%
	Time	**Black**	**White**	**Mylar**	**% W/B**	**% M/B**
Direct Side	10/09/2014 8:51	3.71E-04	3.70E-04	3.69E-04	0.20%	0.53%
	10/09/2014 11:52	3.01E-04	3.01E-04	3.04E-04	0.10%	0.79%

D. CONCLUSIONS AND FUTURE WORK

A simulation procedure has been established to perform a stray light analysis in order to estimate the uncertainty magnitude of δS^{A}_{Direct} and δS^{A}_{Diff} corresponding to direct and diffuse contribution of the lander reflections to the final signal. In addition, optical tests have been performed with a representative mock-up of the lander to check out the validation of the simulation. Finally, we have verified the correct performance for the simulation according to the results of experimental measurements.

As future work, we plan to perform simulations with different kind of Sky-Radiance and Sky-Conditions in order to improve the knowledge about the optical behavior of uncertainty introduced by the lander reflections.

E. ACKNOWLEDGMENTS

Part of this work has been funded with the help of the Spanish National Research, Development and Innovation Program, through the grants AYA2011-29967-C05-01 and ESP2014-54256-C4-3-R.

[1] V. Apestigue, J.J. Jiménez et al "2014 DREAMS-SIS: A Miniature Instrument for the Measurement of Atmospheric Optical Depth on ExoMars 2016 EDM". *International Workshop on Instrumentation for Planetary Missions*, Greenblet, Maryland (IPM-2014).
[2] I.Arruego, et al., "DREAMS-SIS, the solar Irradiance Sensor on-board the ExoMars 2016 Lander: concept, design and operating principles". unpublished
[3] F. Esposito, et al., DREAMS for the ExoMars 2016 mission: a suite of sensors for the characterization of Martian environment, *European Planetary Science Congress, (2013).*
[4] http://exploration.esa.int/mars/48898-edm-science-payload
[5] Eric C. Fest. "*Stray Light Analysis and Control"* ISBN 978-0-8194-9325-5 , Published by SPIE, 2013.
[6] Donal Bédard, Gregg A. Wade, Andrew Jolley, "Interpretation of spectrometric measurements of active geostationary satellites". *Proceedings of the Advanced Maui Optical and Space Surveillance Technologies Conference*, Hawaii, September 9-12, 2014.
[7] Lu Bai, Zhensen Wu, Yunhua Cao, Xun Huang, "Spectral scattering characteristics of space target in near-UV to visible bands" , *Optics Express*, Vol.22, No.7, (April 2014).
[8] J.J. Jimenez, F.J. Alvarez-Ríos, et al., "Calibration OGSE for multichannel radiometer for Mars atmosphere studies". *International conference on space Optics (ICSO).* Biarritz, France (2016).
[9] R.Perez, R. Seals, and J. Michalsky. "Modelling Skylight Angular Luminance Distribution from Routine Irradiance Measurements". *Journal of the Illuminating Engineering Society*, Vol. 22, Iss.1, 1993.
[10] Y.Uetani, "Spatial distribution of daylight-CIE standard general Sky", Vienna, Austria, 2003.
[11] C. Gueymard, "Simple Model of the Atmospheric Radiative Transfer of Sunshine, version 2 (SMARTS2): Algorithms description and performance assessment". *Report FSEC-PF-270-95, Florida Solar Energy Center* (1995).
[12] C. Gueymard, "SMARTS Code, version 2.9.5, User's Manual" *Solar Consulting Services, USA*, December 2005.